# Synthesis of Vector Parasites in Finite Element Maxwell Solutions

Daniel R. Lynch, Keith D. Paulsen, and William E. Boyse

*Abstract*— **Closed-form solutions to driven boundary value problems are obtained for the discrete finite element forms of the double-curl, penalty, and Helmholtz equations, as realized on simple $C^\circ$ bilinear elements. The solutions are expressed as a composite of physical and spurious vector modes, and are qualitatively similar to numerical solutions reported on more complex geometries. The findings reveal the critical role of discrete boundary conditions in determining the strength of the spurious modes; the overall superiority of the Helmholtz weak form; and the importance of proper boundary conditions for its successful use. In particular, one blend of normal and tangential conditions which appears well-posed is shown to be inappropriate; and a simple alternative is shown to work well.**

## I. Introduction

THE occurrence of spurious vector modes in finite element solutions to Maxwell's equations has been reported for over 20 years [4], [5], and is still a topic of considerable interest today (e.g., [2], [6], and [1]). Their elusive but occasionally overwhelming presence has significantly inhibited the electromagnetic application of the FEM. In particular, vector applications using conventional, scalar FEM bases (e.g., $C^\circ$ linear elements) have been especially vulnerable. Since these bases are of considerable practical importance, the control of vector parasites remains a major concern [9], [3].

In a previous paper [7], we introduced dispersion analysis of the discretized equations as a tool in the diagnosis and design of numerical methods. This analysis treats an infinite 2-D lattice of square bilinear elements, and exposes the modal structure of the discrete solution. Spurious vector modes of 3 types are readily identifiable in various discretizations. Analysis of the mode properties (e.g., their divergence and curl) supports conclusions about the presence of parasites in driven problems. The role of boundary conditions is highlighted in the synthesis of physical and spurious modes, relying on general arguments. However, the actual discrete equations used at a mesh termination, and the details of boundary condition enforcement, have not been analyzed.

Our purpose here is to examine in detail the discrete boundary conditions and the various options for their enforcement on finite grids. This allows the expression of closed-form discrete solutions to driven boundary-value problems on a finite mesh.

Manuscript received September 21, 1992; revised November 30, 1992. This work was supported by the U.S. National Institutes of Health under Grants NCI CA 37245 and NCI CA 45357; and NSF Grant ECS-9218750

D. R. Lynch and K. D. Paulsen are with Dartmouth College, Hanover, NH 03755-8000.

W. E. Boyse is with Lockheed Palo Alto Research Laboratories, Palo Alto, CA 94302.

IEEE Log Number 9210231.

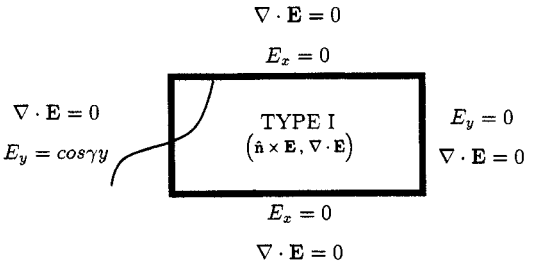


Fig. 1. The Type I problem. Dirichlet conditions are enforced on tangential $\boldsymbol{E}$; natural normal conditions.

Of course, the solutions are restricted to simple geometry; but the analysis clarifies the role of boundary conditions in dictating the final synthesis of spurious and physical modes in the driven solution.

## II. Analytic Solutions

We employ two simple test cases with $\boldsymbol{E}$ in the $(xy)$ plane. Both are governed by the source-free Maxwell equations

$$\nabla \times \boldsymbol{E} = i\omega\mu\boldsymbol{H} \tag{1}$$

$$\nabla \times \boldsymbol{H} = -i\omega\epsilon\boldsymbol{E}. \tag{2}$$

In the first problem, boundary conditions are prescribed on tangential $\boldsymbol{E}$, as in Fig. 1. We refer to these as "Type I" boundary conditions relative to $\boldsymbol{E}$. In the second case, Fig. 2, conditions are prescribed on tangential $\boldsymbol{H}$, which are converted into "Type II" conditions on $\boldsymbol{E}$, specifically,

$$\hat{\boldsymbol{n}} \times \nabla \times \boldsymbol{E} = i\omega\mu\hat{\boldsymbol{n}} \times \boldsymbol{H} \tag{3}$$

and (optionally)

$$\hat{\boldsymbol{n}} \cdot \boldsymbol{E} = -\frac{1}{i\omega\epsilon}\hat{\boldsymbol{n}} \cdot \nabla \times \boldsymbol{H} \tag{4}$$

both of which may be computed from the specified $\hat{\boldsymbol{n}} \times \boldsymbol{H}$. Use of (3) alone or in conjunction with $\nabla \cdot \boldsymbol{E} = 0$ will be referred to as "Type IIa;" use of (3) and (4) will be referred to as "Type IIb."

We seek solutions of the form

$$\begin{Bmatrix} E_x(x,y) \\ E_y(x,y) \end{Bmatrix} = \begin{Bmatrix} E_{xo} \\ E_{yo} \end{Bmatrix} e^{i(\sigma x + \gamma y)}. \tag{5}$$

With $\gamma$ and $\omega$ given, the dispersion relation gives

$$\sigma = +\sqrt{k^2 - \gamma^2} \tag{6}$$

$$k^2 \equiv \omega^2\mu\epsilon. \tag{7}$$

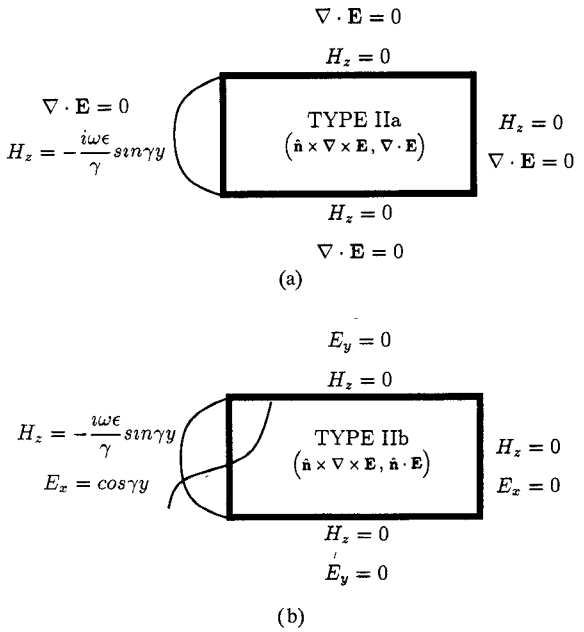


Fig. 2. (a) The Type II problem with all natural boundary conditions. (b) The Type II problem with the same natural tangential conditions but with Dirichlet normal conditions.

The condition $\nabla \cdot \boldsymbol{E} = 0$ also provides the modal information

$$f \equiv \frac{E_{xo}}{E_{yo}} = \frac{-\gamma}{\sigma} . \tag{8}$$

The solution is then a synthesis of forward-and backward-traveling waves

$$\begin{Bmatrix} E_x \\ E_y \end{Bmatrix} = \frac{\alpha^+}{2} \begin{Bmatrix} f \\ 1 \end{Bmatrix} e^{i(\sigma x + \gamma y)} + \frac{\alpha^-}{2} \begin{Bmatrix} -f \\ 1 \end{Bmatrix} e^{i(\sigma x - \gamma y)} + \frac{\beta^+}{2} \begin{Bmatrix} -f \\ 1 \end{Bmatrix} e^{i(-\sigma x + \gamma y)} + \frac{\beta^-}{2} \begin{Bmatrix} f \\ 1 \end{Bmatrix} e^{i(-\sigma x - \gamma y)} . \tag{9}$$

*Type I Problem:* The top and bottom boundary conditions require $\alpha^+ = \alpha^-$ and $\beta^+ = \beta^-$; solution then condenses to trigonometric modes

$$\begin{Bmatrix} E_x \\ E_y \end{Bmatrix} = \alpha e^{\imath\sigma x} \begin{Bmatrix} if \sin\gamma y \\ \cos\gamma y \end{Bmatrix} + \beta e^{-\imath\sigma x} \begin{Bmatrix} -if \sin\gamma y \\ \cos\gamma y \end{Bmatrix} . \tag{10}$$

Finally, application of the left and right boundary conditions on $E_y$ gives

$$\begin{bmatrix} 1 & 1 \\ e^{\imath\sigma L_x} & e^{-i\sigma L_x} \end{bmatrix} \begin{Bmatrix} \alpha \\ \beta \end{Bmatrix} = \begin{Bmatrix} 1 \\ 0 \end{Bmatrix} \tag{11}$$

which, for nonsingular conditions, gives a unique solution for the forward-and backward-propagating wave amplitudes $\alpha$ and $\beta$.

*Type Ii Problem:* Applying top and bottom conditions to (9) requires $\alpha^+ = -\alpha^-$ and $\beta^+ = -\beta^-$; this solution then condenses to the alternate trigonometric modes

$$\begin{Bmatrix} E_x \\ E_y \end{Bmatrix} = \alpha e^{\imath\sigma x} \begin{Bmatrix} f \cos\gamma y \\ i \sin\gamma y \end{Bmatrix} + \beta e^{-\imath\sigma x} \begin{Bmatrix} -f \cos\gamma y \\ i \sin\gamma y \end{Bmatrix} \tag{12}$$

and the left and right conditions on $E_x$ then determine $\alpha$ and $\beta$

$$\begin{bmatrix} f & -f \\ fe^{i\sigma L_x} & -fe^{-\imath\sigma L_x} \end{bmatrix} \begin{Bmatrix} \alpha \\ \beta \end{Bmatrix} = \begin{Bmatrix} 1 \\ 0 \end{Bmatrix} . \tag{13}$$

Because of their natural utility, we identify modes of the form (10) as "Type I" trigonometric modes, and those of form (12) as "Type II."

## III. Difference Equations

We consider the so-called "penalty" form of the Maxwell equations, for constant coefficients

$$\nabla \times (\nabla \times \boldsymbol{E}) - p\nabla(\nabla \cdot \boldsymbol{E}) - k^2 \boldsymbol{E} = 0 \tag{14}$$

and the associated weak form [9], [3]

$$\langle (\nabla \times \boldsymbol{E}) \times \nabla\phi_i \rangle + p\langle (\nabla \cdot \boldsymbol{E}) \nabla\phi_i \rangle - \langle k^2 \boldsymbol{E}\phi_i \rangle = -\oint \hat{\boldsymbol{n}} \times (\nabla \times \boldsymbol{E})\phi_i \, ds + p \oint \hat{\boldsymbol{n}} \nabla \cdot \boldsymbol{E}\phi_i \, ds \tag{15}$$

in which $\langle\,\rangle$ is the domain integral, $\oint ds$ is the integral on the enclosing surface, and $\phi_i(x, y)$ is a scalar weighting function. For $p = 0$, we have the conventional double-curl equation; $p = 1$ gives the "expanded weak form" advocated by Paulsen and Lynch [9] and Boyse *et al.* [3]. On the interior, the latter is identical to the Helmholtz weak form for the scalar components of $\boldsymbol{E}$ individually.

We examine the discrete from of (15) which would be realized on a uniform grid of square bilinear elements using the Galerkin method.

*Interior Conditions:* For all interior $\phi_i$, the difference expressions developed previously in [7, Table I and equation (20)] apply. For exponential solutions of the form (5), these interior difference equations take the form (16) below.
(The discretization factors $A, B, C$ defined in [7] are repeated here in Table II for convenience. Note that each of these factors approaches unity with mesh refinement.) All interior equations (16) are satisfied simultaneously by satisfaction of the dispersion relation

$$\left(k^2 - p\kappa^2\right)\left(k^2 - \kappa^2\right) + (1-p)^2\epsilon^2 = 0 \tag{17a}$$

$$\begin{bmatrix} A_x C_y^2 \gamma^2 + pA_y C_x^2 \sigma^2 - A_x A_y k^2 & -(1-p) B_y B_x \gamma\sigma \\ -(1-p) B_x B_y \sigma\gamma & A_y C_x^2 \sigma^2 + pA_x C_y^2 \gamma^2 - A_x A_y k^2 \end{bmatrix} \begin{Bmatrix} E_x \\ E_y \end{Bmatrix} = \begin{Bmatrix} 0 \\ 0 \end{Bmatrix} \tag{16}$$

TABLE I
DIFFERENCE OPERATORS AND EQUATIONS AT A MESH BOUNDARY

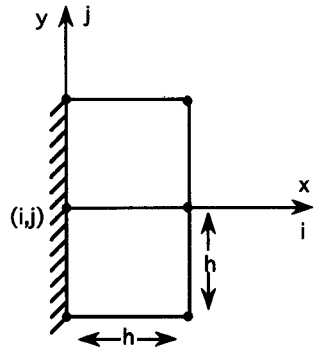


$$\frac{1}{h^2}\left[\langle(\nabla\times\boldsymbol{E})\times\nabla\phi_{ij}\rangle+p\langle(\nabla\cdot\boldsymbol{E})\nabla\phi_{ij}\rangle-\langle k^2\boldsymbol{E}\phi_{ij}\rangle\right]=\begin{bmatrix}-\frac{1}{2}\frac{\delta_y^2}{h^2}S'_x-\frac{k^2}{2}S'_xS_y-\frac{p}{h^2}\Delta_xS_y & \frac{\delta_y}{2h}\left[\frac{\Delta_x}{2h}-p\frac{S^*_x}{h}\right]\\ \frac{\delta_y}{2h}\left[\frac{S^*_x}{h}-p\frac{\Delta_x}{2h}\right] & -\frac{\Delta_x}{h^2}S_y-\frac{k^2}{2}S'_xS_y-\frac{p}{2}\frac{\delta_y^2}{h^2}S'_x\end{bmatrix}\begin{Bmatrix}E_{xij}\\E_{yij}\end{Bmatrix}$$

| | |
|---|---|
| $\delta_yU_{ij}\equiv U_{i,j+1}-U_{i,j-1}$ | first centered difference |
| $\delta_y^2U_{ij}\equiv U_{i,j+1}-2U_{i,j}+U_{i,j-1}$ | second centered difference |
| $\Delta_xU_{i,j}\equiv U_{i+1,j}-U_{i,j}$ | first forward difference |
| $S_yU_{ij}\equiv\frac{1}{6}(U_{i,j+1}+4U_{i,j}+U_{i,j-1})$ | Simpson's rule average |
| $S'_xU_{ij}\equiv\frac{1}{3}(U_{i+1,j}+2U_{ij})$ | forward average |
| $S^*_xU_{ij}\equiv\frac{1}{2}(U_{i+1,j}+U_{ij})$ | forward average |

with

$$\kappa^2\equiv\frac{C_x^2\sigma^2}{A_x}+\frac{C_y^2\gamma^2}{A_y} \tag{17b}$$

$$\epsilon^2\equiv\sigma^2\gamma^2\left(\frac{C_x^2}{A_x}\frac{C_y^2}{A_y}-\frac{B_x^2}{A_x^2}\frac{B_y^2}{A_y^2}\right). \tag{17c}$$

From (16) we also have the modal characteristic

$$f\equiv\frac{E_x}{E_y}=\frac{(1-p)B_yB_x\gamma\sigma}{A_xC_y^2\gamma^2+pA_yC_x^2\sigma^2-A_xA_yk^2}=\frac{A_yC_x^2\sigma^2+pA_xC_y^2\gamma^2-A_xA_yk^2}{(1-p)B_xB_y\sigma\gamma}. \tag{18}$$

Equations (17) and (18) completely describe the solution to (16). There are no other requirements imposed by the interior difference equations. (For $p=1$, $f$ remains undefined by (16). It is determined by the boundary conditions; see below.)

The discrete dispersion relation (17) allows two values $\sigma_1^2,\sigma_2^2$ for each combination of $k^2$ and $\gamma^2$, as developed in [7]. Each supports a solution analogous to (9). The general solution is therefore the superposition of 8 exponential modes

$$\begin{Bmatrix}E_x\\E_y\end{Bmatrix}=\frac{\alpha_1^+}{2}\begin{Bmatrix}f_1\\1\end{Bmatrix}e^{i(\sigma_1x+\gamma y)}+\frac{\alpha_1^-}{2}\begin{Bmatrix}-f_1\\1\end{Bmatrix}e^{i(\sigma_1x-\gamma y)}+\frac{\beta_1^+}{2}\begin{Bmatrix}-f_1\\1\end{Bmatrix}e^{i(-\sigma_1x+\gamma y)}+\frac{\beta_1^-}{2}\begin{Bmatrix}f_1\\1\end{Bmatrix}e^{i(-\sigma_1x-\gamma y)}+\frac{\alpha_2^+}{2}\begin{Bmatrix}f_2\\1\end{Bmatrix}e^{i(\sigma_2x+\gamma y)}+\frac{\alpha_2^-}{2}\begin{Bmatrix}-f_2\\1\end{Bmatrix}e^{i(\sigma_2x-\gamma y)}+\frac{\beta_2^+}{2}\begin{Bmatrix}-f_2\\1\end{Bmatrix}e^{i(-\sigma_2x+\gamma y)}+\frac{\beta_2^-}{2}\begin{Bmatrix}f_2\\1\end{Bmatrix}e^{i(-\sigma_2x-\gamma y)}. \tag{19a}$$

As in [7], we identify $\pm\sigma_1$ as the spurious modes, and $\pm\sigma_2$ as the nearly correct physical modes.

For the special case $p=1$ (Helmholtz equation), the two dispersion surfaces merge, and $f$ is undefined by the interior equations. There are thus only four exponential modes, but each has two degrees of freedom, i.e., $E_x$ and $E_y$ are uncoupled. For compatibility with (19a), these may be expressed as

$$\begin{Bmatrix}E_x\\E_y\end{Bmatrix}=\frac{\alpha^+}{2}\begin{Bmatrix}f_\alpha^+\\1\end{Bmatrix}e^{i(\sigma x+\gamma y)}+\frac{\alpha^-}{2}\begin{Bmatrix}-f_\alpha^-\\1\end{Bmatrix}e^{i(\sigma x-\gamma y)}+\frac{\beta^+}{2}\begin{Bmatrix}-f_\beta^+\\1\end{Bmatrix}e^{i(-\sigma x+\gamma y)}+\frac{\beta^-}{2}\begin{Bmatrix}f_\beta^-\\1\end{Bmatrix}e^{i(-\sigma x-\gamma y)} \tag{19b}$$

with 8 unknowns $\alpha,\beta,f$.

*Boundary Conditions:* At boundaries, (16) does not govern. Rather, one-sided difference equations are enforced, as displayed in Table I. Unlike their centered homogeneous counterparts on the mesh interior, these are in general inhomogenous, with the boundary integral terms driving and/or correcting the one-sided differences.

A special feature of the boundary difference equations is their *transparency* to certain select trigonometric modes. Consider the various one-sided difference operators in Table I. For a solution which is symmetric across the boundary, we have the following identities among the forward and centered difference operators:

$$S'_x\equiv S_x\quad\text{and}\quad 2\Delta_x\equiv\delta_x^2$$

and for a function which is antisymmetric, we have

$$\Delta_x\equiv 2S^*_x\equiv\frac{1}{2}\delta_x.$$

Now consider the normal ($x$) equation in Table I, in homogeneous form. A solution of the form

$$\begin{Bmatrix} E_x \\ E_y \end{Bmatrix} = \begin{Bmatrix} U(y)\cos ax \\ V(y)\sin bx \end{Bmatrix}$$

reduces this equation, term by term, to its centered counterpart on the interior of the mesh. (For the latter, see [7, equation (20) and Table 1]). Solutions with this symmetry which satisfy the interior equations therefore automatically satisfy the homogeneous form of this boundary equation— it adds no additional constraints. It is as if the mesh boundary were not present at all. We refer to this property as "transparency" of a boundary condition to a particular mode. (Note that the $y$-equation is *not* transparent to this mode.)

Generalizing to normal, tangential coordinates $(n, s)$, we have

- the discrete normal BC is transparent to modes of the form

$$\begin{Bmatrix} E_n \\ E_s \end{Bmatrix} = \begin{Bmatrix} U(s)\cos an \\ V(s)\sin bn \end{Bmatrix}.$$

The same reasoning with the $y$-equation in Table I leads to the dual conclusion

- the discrete tangential BC is transparent to modes of the form

$$\begin{Bmatrix} E_n \\ E_s \end{Bmatrix} = \begin{Bmatrix} U(s)\sin an \\ V(s)\cos bn \end{Bmatrix}.$$

These properties will be important in the mode synthesis below.

For general exponential solutions of the form (5), we define the one-sided discretization factors $A', A^*, B'$, as in Table II. Like their interior counterparts, each of these factors approaches unity with mesh refinement. Using these, we transform the boundary conditions at the left end of the mesh and obtain equation (20a) below. The summation in (20a) is over all *exponential* modes[1], and highlights the role of the boundary conditions in ultimate mode synthesis. Analogous relations obtain at the other boundaries—for example, at the bottom boundary we have equation (20b) below. These will be further modified by the imposition of various boundary conditions, as discussed next. For a given problem, then, we have the general solution (19), subject to (20) rotated and modified appropriately on the four boundaries. These completely determine the discrete solution.

TABLE II
DISCRETIZATION FACTORS FOR SOLUTIONS OF EXPONENTIAL FORM $U \sim e^{i(\sigma x+\gamma y)}$. NOTE THAT ALL $A, B$, AND $C$ FACTORS APPROACH UNITY AS $h \to 0$

$$\begin{array}{ll} A_x \equiv \frac{4+2\cos\sigma h}{6} & A'_x \equiv \frac{2+e^{i\sigma h}}{3} \\ B_x \equiv \frac{\sin\sigma h}{\sigma h} & A^*_x \equiv \frac{1+e^{i\sigma h}}{2} \\ C_x \equiv \frac{\sin\sigma h/2}{\sigma h/2} & B'_x \equiv \frac{e^{i\sigma h}-1}{i\sigma h} \\ & A^*_x \equiv 1 + \frac{i\sigma h B'_x}{2} \end{array}$$

$$\begin{aligned} \frac{\delta_y^2 U_{ij}}{h^2} &= -\gamma^2 C_y^2 U_{ij} \\ \frac{\delta_y U_{ij}}{2h} &= i\gamma B_y U_{ij} \\ \frac{\Delta_x U_{ij}}{h} &= i\sigma B'_x U_{ij} \end{aligned}$$

[1] When summing over trigonometric modes, care must be exercised to break them into their component exponentials and then reassemble. An alternate, equivalent summation may be made over the trignometric modes per se. In this case, the product $\gamma\cos\gamma y$ produces $\gamma i \sin\gamma y$, and vice versa.

$$\sum_l \begin{bmatrix} \frac{1}{2}A'_xC_y^2\gamma^2 - \frac{p}{h}i\sigma B'_xA_y - \frac{1}{2}A'_xA_yk^2 & i\gamma B_y\left(\frac{i}{2}\sigma B'_x - \frac{p}{h}A^*_x\right) \\ i\gamma B_y\left(\frac{1}{h}A^*_x - \frac{ip}{2}\sigma B'_x\right) & \frac{p}{2}A'_xC_y^2\gamma^2 - \frac{1}{h}i\sigma B'_xA_y - \frac{1}{2}A'_xA_yk^2 \end{bmatrix}_l \begin{Bmatrix} E_x \\ E_y \end{Bmatrix}_l = -\frac{1}{h^2}\begin{Bmatrix} p\oint\left(\frac{\partial E_x}{\partial x} + \frac{\partial E_y}{\partial y}\right)\phi_i\,ds \\ \oint\left(\frac{\partial E_y}{\partial x} - \frac{\partial E_x}{\partial y}\right)\phi_i\,ds \end{Bmatrix}. \quad (20a)$$

$$\sum_l \begin{bmatrix} \frac{p}{2}A'_yC_x^2\sigma^2 - \frac{1}{h}i\gamma B'_yA_x - \frac{1}{2}A'_yA_xk^2 & i\sigma B_x\left(\frac{1}{h}A^*_y - \frac{ip}{2}\gamma B'_y\right) \\ i\sigma B_x\left(\frac{i}{2}\gamma B'_y - \frac{p}{h}A^*_y\right) & \frac{1}{2}A'_yC_x^2\sigma^2 - \frac{p}{h}i\gamma B'_yA_x - \frac{1}{2}A'_yA_xk^2 \end{bmatrix}_l \begin{Bmatrix} E_x \\ E_y \end{Bmatrix}_l = -\frac{1}{h^2}\begin{Bmatrix} -\oint\left(\frac{\partial E_y}{\partial x} - \frac{\partial E_x}{\partial y}\right)\phi_i\,ds \\ p\oint\left(\frac{\partial E_x}{\partial x} + \frac{\partial E_y}{\partial y}\right)\phi_i\,ds \end{Bmatrix}. \quad (20b)$$

## IV. Mode Synthesis—Type I Problem

In the Type I case, the tangential component of (20) would be discarded in favor of direct specification of $\boldsymbol{E}\cdot\boldsymbol{t}'$; and $\nabla\cdot\boldsymbol{E}=0$ would be set to zero in the boundary integral. On the left boundary, this gives equation (21a) (below); and on the bottom boundary, equation (21b) (below). The top and bottom BC's are exactly satisfied by reduction of the general solution (19a) to Type I trigonometric modes as in (10)

$$\begin{Bmatrix} E_x \\ E_y \end{Bmatrix} = \alpha_1 e^{i\sigma_1 x}\begin{Bmatrix} if_1\sin\gamma y \\ \cos\gamma y \end{Bmatrix} + \beta_1 e^{-i\sigma_1 x}\begin{Bmatrix} -if_1\sin\gamma y \\ \cos\gamma y \end{Bmatrix} + \alpha_2 e^{i\sigma_2 x}\begin{Bmatrix} if_2\sin\gamma y \\ \cos\gamma y \end{Bmatrix} + \beta_2 e^{-i\sigma_2 x}\begin{Bmatrix} -if_2\sin\gamma y \\ \cos\gamma y \end{Bmatrix}. \tag{22}$$

In fact, each of these four modes *independently* satisfies the top and bottom conditions, despite the one-sidedness of the difference equations. For the tangential $(x)$ component of (21b), this is obvious—the Dirichlet condition is effectively transparent to these modes. For the normal $(y)$ component, its transparency to Type I modes has been established above. The BC's are not, however, transparent to Type II modes, and as a consequence their net effect is to eliminate these unwanted Type II modes. *These BC's at top and bottom are therefore perfectly invisible, ideal mesh terminations for this problem.* They do not, however, discriminate between physical and spurious Type I modes. *The critical determinants of physical/spurious mode synthesis in this problem are therefore the left and right BC's.*

It is useful to consider only the forward-propagating modes

$$\begin{Bmatrix} E_x \\ E_y \end{Bmatrix} = \alpha_1 e^{i\sigma_1 x}\begin{Bmatrix} if_1\sin\gamma y \\ \cos\gamma y \end{Bmatrix} + \alpha_2 e^{i\sigma_2 x}\begin{Bmatrix} if_2\sin\gamma y \\ \cos\gamma y \end{Bmatrix} \tag{23}$$

and enforce only the left BC (21a). For $E_y$, we have

$$\alpha_1+\alpha_2=1 \tag{24}$$

and clearly either mode would suffice in isolation. However, neither of the modes alone will satisfy the $x$-component of (21a). For example, substitution of mode 2 alone would require

$$e^{i\sigma_2 x}\left(\frac{1}{2}A'_xC_y^2\gamma^2-\frac{p}{h}i\sigma B'_xA_y-\frac{1}{2}A'_xA_yk^2\right)_2\cdot(f_2-f'_2)i\sin\gamma_y=0 \tag{25a}$$

with $f'_2$ being the mode shape preferred by the boundary equation (21a) for Type I modes

$$f'_2=\left(\frac{-i\gamma B_y\left(\frac{i}{2}\sigma B'_x-\frac{p}{h}A^*_x\right)}{\frac{1}{2}A'_xC_y^2\gamma^2-\frac{p}{h}i\sigma B'_xA_y-\frac{1}{2}A'_xA_yk^2}\right)_2\neq f_2. \tag{25b}$$

Equation (25a) cannot be satisfied as it stands: $f'_2\neq f_2$ for any finite mesh. Unlike the top and bottom BC's, we have an inherent clash between the interior and boundary equations. As a result, both modes must be blended to meet the left BC

$$\left[\alpha_1 e^{i\sigma_1 x}\left(\frac{1}{2}A'_xC_y^2\gamma^2-\frac{p}{h}i\sigma B'_xA_y-\frac{1}{2}A'_xA_yk^2\right)_1\cdot(f_1-f'_1)+\alpha_2 e^{i\sigma_2 x}\left(\frac{1}{2}A'_xC_y^2\gamma^2-\frac{p}{h}i\sigma B'_xA_y-\frac{1}{2}A'_xA_yk^2\right)_2\cdot(f_2-f'_2)\right]i\sin\gamma y=0 \tag{26}$$

evaluated at $x=0$. The final modal mix is then

$$\frac{\alpha_1}{\alpha_2}=-\frac{\left(\frac{1}{2}A'_xC_y^2\gamma^2-\frac{p}{h}i\sigma B'_xA_y-\frac{1}{2}A'_xA_yk^2\right)_2(f_2-f'_2)}{\left(\frac{1}{2}A'_xC_y^2\gamma^2-\frac{p}{h}i\sigma B'_xA_y-\frac{1}{2}A'_xA_yk^2\right)_1(f_1-f'_1)} \tag{27}$$

For $p=0$, this reduces to

$$\frac{\alpha_1}{\alpha_2}=-\frac{(A'_x)_2(f_2-f'_2)}{(A'_x)_1(f_1-f'_1)} \tag{28}$$

which is a remarkably simple result for the relative strength of the parasite! To the extent that $f-f'$ is $o(\sigma h)$, the mode with smaller $|\sigma|$ will dominate.

Examination of the dispersion curves in [7, Fig. 6] shows clearly that under some circumstances $|\sigma_1|$ (the parasite) is comparable to or smaller than $|\sigma_2|$. Fig. 3 displays (28) as a function of $(\gamma h)^2$ for fixed values of $(kh)^2$, which reveals that the parasitic mode can indeed dominate the solution for well-resolved meshes.[2] A visually dramatic example of the effect of the parasite is shown in Fig. 4 where $(kh)^2=0.001$ and $(\gamma h)^2=0.0987$, which yields an $\alpha_1/\alpha_2$ ratio near unity. For these parameters, the $p=0$ modal solution has

[2]Recall that the 10 nodes/wavelength cutoff corresponds to $(kh)^2$ and $(\gamma h)^2$ values of 0.4; see [7, Fig. 1].

$$\sum_l\begin{bmatrix} \frac{1}{2}A'_xC_y^2\gamma^2-\frac{p}{h}i\sigma B'_xA_y-\frac{1}{2}A'_xA_yk^2 & i\gamma B_y\left(\frac{i}{2}\sigma B'_x-\frac{p}{h}A^*_x\right) \\ 0 & 1 \end{bmatrix}_l\begin{Bmatrix} E_x \\ E_y \end{Bmatrix}_l=\begin{Bmatrix} 0 \\ \cos\gamma y \end{Bmatrix} \tag{21a}$$

$$\sum_l\begin{bmatrix} 1 & 0 \\ i\sigma B_x\left(\frac{i}{2}\gamma B'_y-\frac{p}{h}A^*_y\right) & \frac{1}{2}A'_yC_x^2\sigma^2-\frac{p}{h}i\gamma B'_yA_x-\frac{1}{2}A'_yA_xk^2 \end{bmatrix}_l\begin{Bmatrix} E_x \\ E_y \end{Bmatrix}_l=\begin{Bmatrix} 0 \\ 0 \end{Bmatrix}. \tag{21b}$$

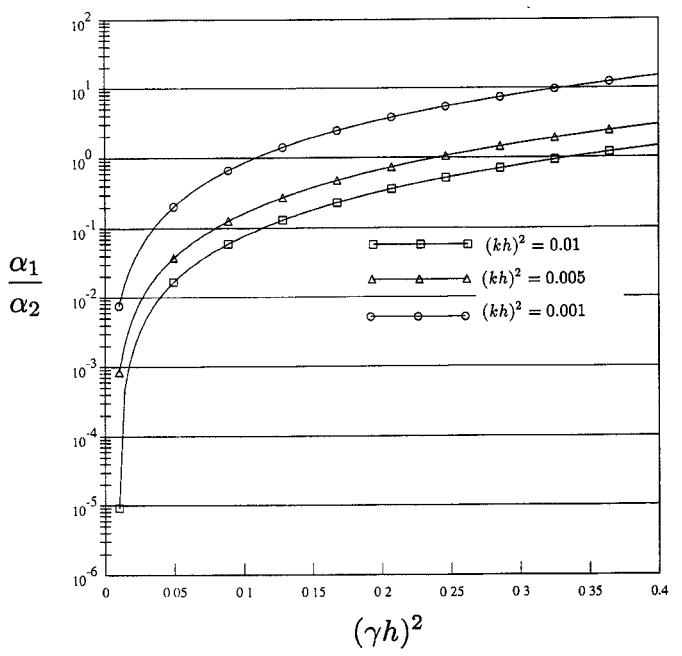


Fig. 3. Relative strength of the spurious mode for the $p = 0$ Type I problem.

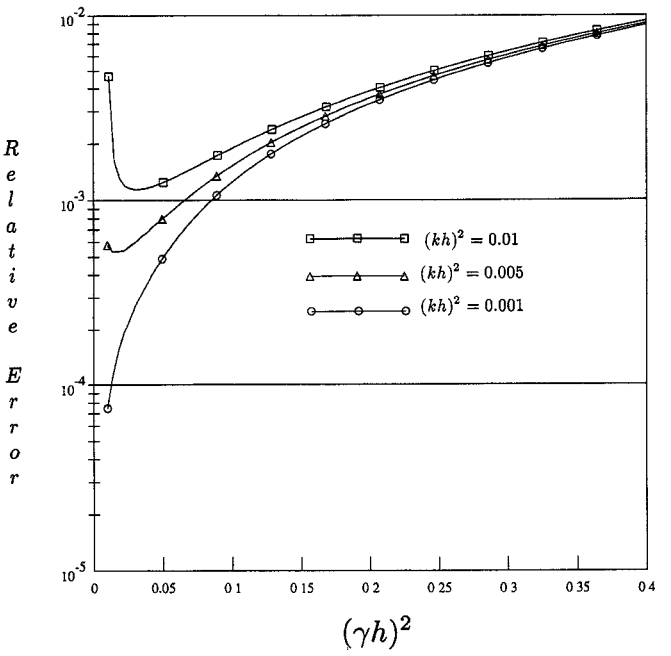


Fig. 5. Relative error in $f$ for the $p = 1$ Type I problem.

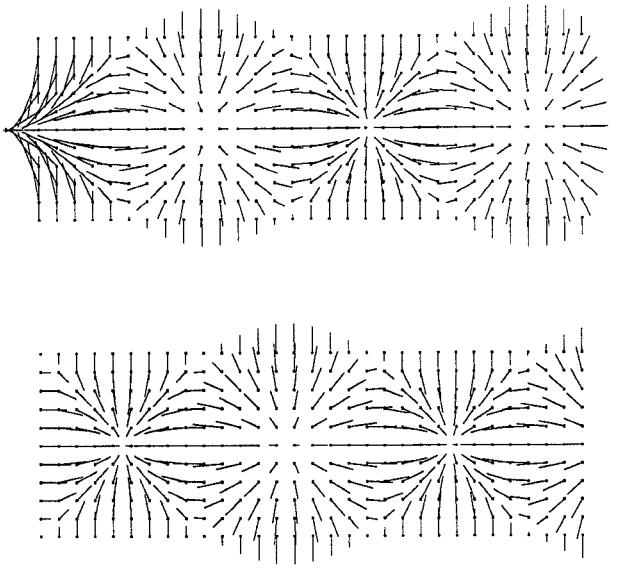

Fig. 4. Vector plot of the *Real* (top) and *Imaginary* (bottom) parts of the $p = 0$ Type I problem solution when $(kh)^2 = 0.001$ and $(\gamma h)^2 = 0.0987$.

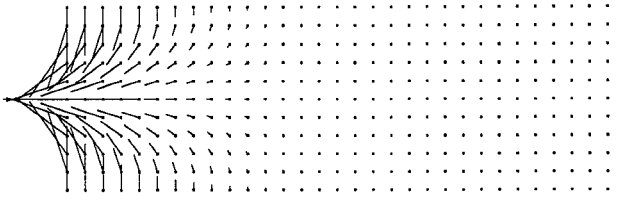

Fig. 6. Same as Fig. 4 for $p = 1$. The *Real* part is shown; the *Imaginary* part is zero.

$\alpha_1 = 0.4517$, $\sigma_1 h = 0.3455$, $f_1 = 1.102$, and $\alpha_2 = 0.5483$, $\sigma_2 h = i0.3165$, $f_2 = i1.0092$ in (23)—the solution plotted in Figure 4—whereas the analytic result requires $\alpha = 1.0$, $\sigma h = i0.3126$, and $f = i1.005$.

Clearly the $p = 0$ physical mode is attempting to mimic its analytic counterpart in that it has nearly correct dispersion relation and modal characteristic. Unfortunately, it only comprises about half of the total solution with the other component having completely erroneous propagation and modal characteristics. Fig. 4 is reminiscent of the types of solutions shown by Paulsen and Lynch [9] for more complex heterogeneous problems. Further, Fig. 3 confirms the observations in [7] that when $p = 0$, the spurious solution size generally persists with mesh refinement.

When $p = 1$, $f_1$ and $f_2$ are undefined by the interior equations and the two dispersion surfaces merge. In this case, the BC's determine both $f$ and $\alpha$ (equivalently, $E_x$ and $E_y$) for each of the four modes in (19b). In the Type I problem, a single composite Type I mode of the form

$$\begin{Bmatrix} E_x \\ E_y \end{Bmatrix} = \alpha e^{i\sigma x} \begin{Bmatrix} if \sin \gamma y \\ \cos \gamma y \end{Bmatrix} \tag{29}$$

exactly satisfies the top and bottom BC's for arbitrary $f$ and $\alpha$. The left BC [equation (21a)] determines both $\alpha$ and $f$

$$\alpha = 1 \tag{30}$$

$$f = \frac{i\gamma B_y}{\frac{h}{2} A'_x \left(C_y^2 \gamma^2 - A_y k^2\right) - i\sigma B'_x A_y}. \tag{31}$$

This is an approximation which converges to the exact divergence-free solution $f = -\gamma/\sigma$.

As a measure of fidelity for the $p = 1$ case, Fig. 5 is presented which shows the relative error in (31) with respect to the analytic $f$ as $(\gamma h)^2$ varies for fixed values of $(kh)^2$. Fig. 6 shows the discrete solution when $p = 1$ for the same set of $(\gamma h)^2$ and $(kh)^2$ values used in Fig. 4. In this case, $\sigma h = i0.3152$ and $f = i0.9968$ in (29). The quality of the $p = 1$ solution is clear: $\sigma$ and $f$ are in error by less than 1% relative to their correct values. Comparison of Fig. 6, which is essentially a rendering of the analytic solution, to Fig. 4

provides indisputable evidence of the fatal weakness of the double-curl solution and adds further credibility to the strength of Helmholtz weak forms.

## V. Mode Synthesis—Type II Problem

In the Type IIa case, we have all natural conditions as in (20). In the Type IIb case, $\boldsymbol{E}\cdot\hat{\boldsymbol{n}}$ is specified strongly, and the normal equation discarded. The latter case is simpler and we consider it first.

***Type IIb:*** The Type IIb boundary equations are given in equation (32) (below) for left (a) and bottom (b) cases. Analogous to the Type I problem, the bottom and top BC's are satisfied exactly with Type II trigonometric modes

$$\begin{Bmatrix} E_x \\ E_y \end{Bmatrix} = \alpha_1 e^{i\sigma_1 x}\begin{Bmatrix} f_1\cos\gamma y \\ i\sin\gamma y \end{Bmatrix} + \beta_1 e^{-i\sigma_1 x}\begin{Bmatrix} -f_1\cos\gamma y \\ i\sin\gamma y \end{Bmatrix} + \alpha_2 e^{i\sigma_2 x}\begin{Bmatrix} f_2\cos\gamma y \\ i\sin\gamma y \end{Bmatrix} + \beta_2 e^{-i\sigma_2 x}\begin{Bmatrix} -f_2\cos\gamma y \\ i\sin\gamma y \end{Bmatrix}. \tag{33}$$

Further, each of these modes *independently* satisfies the top and bottom BC's, by virtue of tangential transparency and the Dirichlet condition on the normal field. Finally, these BC's demand the vanishing of the Type I modes. The top and bottom BC's are therefore perfect mesh terminations; they exert no additional influence on Type II modes and cancel all Type I modes. The blend of physical and spurious Type II modes is left undetermined.

Proceeding as in the Type I problem, we synthesize the solution for forward-propagating waves by enforcing the left BC. We define $f''$ as the mode shape preferred by the tangential (y) equation at the left (32a)

$$f'' = -\frac{\frac{p}{2}A'_x C_y^2\gamma^2 - \frac{1}{h}i\sigma B'_x A_y - \frac{1}{2}A'_x A_y k^2}{i\gamma B_y\left(\frac{1}{h}A^*_x - \frac{ip}{2}\sigma B'_x\right)} \tag{34}$$

and obtain equation (35) (below) for the mode strengths. Solution of (35) provides the relative strength of the parasite. For $p = 0$, it is

$$\frac{\alpha_1}{\alpha_2} = \frac{(A^*_x)_2(f_2 - f''_2) - f_2\frac{A_y k^2}{B_y\gamma^2}}{(A^*_x)_1(f_1 - f''_1) - f_1\frac{A_y k^2}{B_y\gamma^2}}. \tag{36}$$

Fig. 7 shows this ratio as a function of $(\gamma h)^2$ for well-resolved $(kh)^2$ values. Interestingly, it remains rather small over the full range of reasonably resolved $(\gamma h)^2$. As a result, the spurious mode does not play a dominant role in determining the total solution for the Type IIb problem of Fig. 2(b). Fig. 8 and 9 show vector plots of the physical and spurious modes separately when $(kh)^2 = 0.001$ and $(\gamma h)^2 = 0.0987$. Fig. 8 (the physical mode) is an excellent representation of the analytic solution having the same nearly correct values of $\sigma_2$ and $f_2$ as in the Type I problem with $\alpha_2 f_2$ nearly unity, whereas Fig. 9 (the parasite) displays the classical erroneous divergence-type behavior. It should be noted that the scale of the solution in Fig. 9 is magnified 200 times relative to Fig. 8 reflecting the small size of $\alpha_1$ compared to $\alpha_2$. While Fig. 9 represents a small portion of the total solution near the left boundary, the physical mode decays; thus, the propagating spurious mode does become the total discrete solution a few mesh lengths away. Further, it has both real and imaginary components, whereas the analytic solution (and the physical discrete mode) is entirely real. Finally, this parasite propagates without decay to the right boundary, no matter how far removed electrically. This introduces an additional non-local BC on a physically local phenomena, and introduces the possibility of spurious mode resonance. These are unwanted properties which can be eliminated when $p = 1$ as shown below.

For the special case $p = 1$, a single Type II mode suffices

$$\begin{Bmatrix} E_x \\ E_y \end{Bmatrix} = \alpha e^{i\sigma x}\begin{Bmatrix} f\cos\gamma y \\ i\sin\gamma y \end{Bmatrix} \tag{37}$$

$$\sum_l \begin{bmatrix} 1 & 0 \\ i\gamma B_y\left(\frac{1}{h}A^*_x - \frac{ip}{2}\sigma B'_x\right) & \frac{p}{2}A'_x C_y^2\gamma^2 - \frac{1}{h}i\sigma B'_x A_y - \frac{1}{2}A'_x A_y k^2 \end{bmatrix}_l \begin{Bmatrix} E_x \\ E_y \end{Bmatrix}_l = \begin{Bmatrix} \cos\gamma y \\ -\frac{1}{\gamma h}A_y k^2\sin\gamma y \end{Bmatrix} \tag{32a}$$

$$\sum_l \begin{bmatrix} \frac{p}{2}A'_y C_x^2\sigma^2 - \frac{1}{h}i\gamma B'_y A_x - \frac{1}{2}A'_y A_x k^2 & i\sigma B_x\left(\frac{1}{h}A^*_y - \frac{ip}{2}\gamma B'_y\right) \\ 0 & 1 \end{bmatrix}_l \begin{Bmatrix} E_x \\ E_y \end{Bmatrix}_l = \begin{Bmatrix} 0 \\ 0 \end{Bmatrix}. \tag{32b}$$

$$\begin{bmatrix} f_1 & f_2 \\ i\gamma B_y\left(\frac{1}{h}A^*_x - \frac{ip}{2}\sigma B'_x\right)_1(f_1 - f''_1) & i\gamma B_y\left(\frac{1}{h}A^*_x - \frac{ip}{2}\sigma B'_x\right)_2(f_2 - f''_2) \end{bmatrix}\begin{Bmatrix} \alpha_1 \\ \alpha_2 \end{Bmatrix} = \begin{Bmatrix} 1 \\ \frac{i}{\gamma h}A_y k^2 \end{Bmatrix} \tag{35}$$

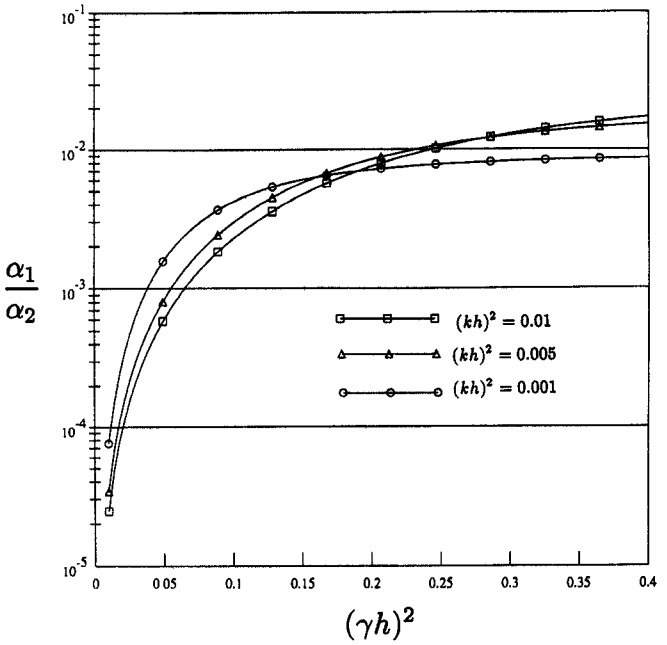


Fig. 7. Relative strength of the spurious mode for the $p = 0$ Type IIb problem.

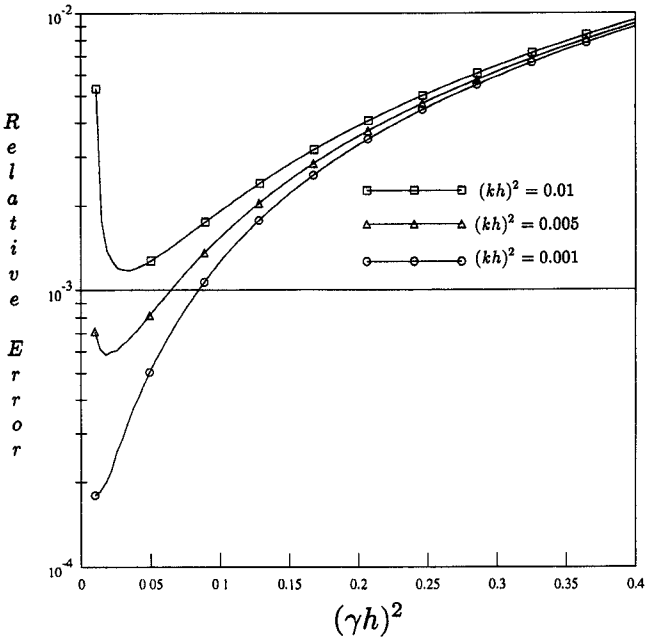


Fig. 10. Relative error in $f$ for the $p = 1$ Type IIb problem.

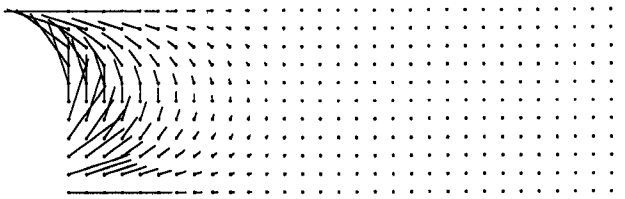

Fig. 8. Vector plot of the physical mode alone for the $p = 0$ Type IIb problem when $(kh)^2 = 0.001$ and $(\gamma h)^2 = 0.0987$.

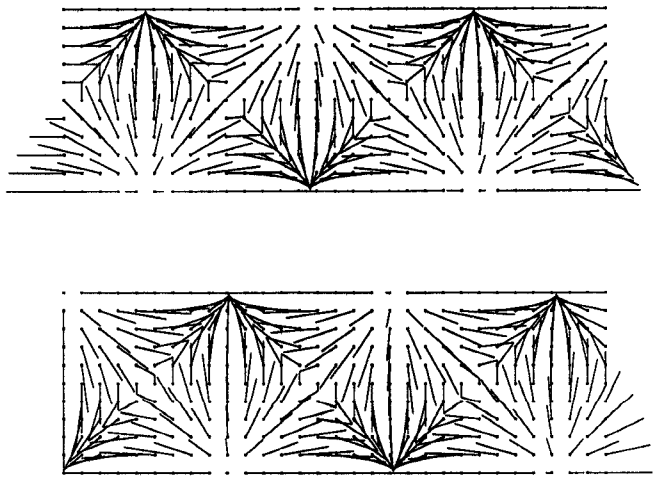

Fig. 9. Same as Fig. 8 for the spurious mode alone: *Real* part (top); *Imaginary* part (bottom). Scale is 200 times that of Fig. 8.

with $\alpha$ and $f$ both determined by the left BC's (32a)

$$\alpha f = 1 \tag{38a}$$

$$i\alpha = \frac{-\frac{1}{\gamma} A_y k^2 + \gamma B_y}{\frac{h}{2} A'_x \left(C_y^2 \gamma^2 - A_y k^2\right) - i\sigma B'_x A_y}. \tag{38b}$$

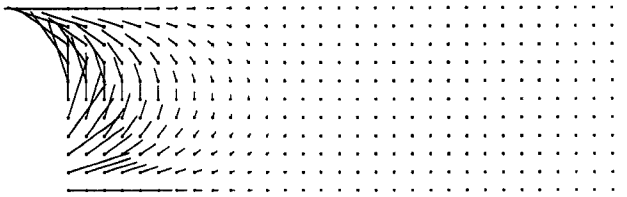

Fig. 11. Vector plot of the $p = 1$ Type IIb problem solution when $(kh)^2 = 0.001$ and $(\gamma h)^2 = 0.0987$. The *Real* part is shown; the *Imaginary* part is zero.

Use of the dispersion relation $k^2 = C_x^2\sigma^2/A_x + C_y^2\gamma^2/A_y$ and rearrangement gives

$$f = \frac{\frac{ih\gamma}{2} A'_x \left(C_y^2\gamma^2 - A_y k^2\right) + \gamma\sigma B'_x A_y}{-\frac{A_y C_x^2 \sigma^2}{A_x} + \gamma^2 \left(B_y - C_y^2\right)}. \tag{38c}$$

which approaches the exact value $-\gamma/\sigma$ with mesh refinement.

As before, the relative error in (38c) with respect to the analytic $f$ is taken as a measure of accuracy of the discrete solution when $p = 1$. This benchmark is plotted in Fig. 10 as a function of $(\gamma h)^2$ when $(kh)^2$ is fixed as done previously. Again, the discrete solution is faithful to the analytic, showing errors in the modal characteristic of less than 1% even for marginally resolved values of $(\gamma h)^2$ in a fashion very similar to the Type I problem. A vector plot of the $p = 1$ solution for the case shown in Fig. 8 and 9 is provided in Fig. 11. The computed results agree to better than 1% with the analytic solution for this specific parameter set.

***Type IIa:*** In this case, we abandon the Dirichlet conditions on the normal field and retain the one-sided approximations to the normal Maxwell equations. To begin with, we apply this

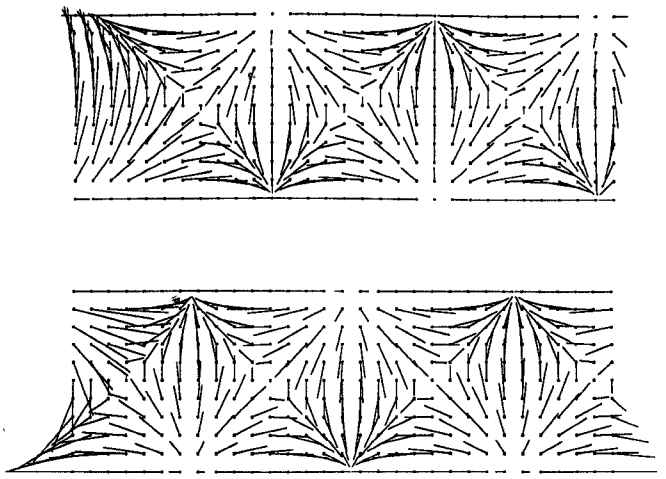

Fig. 12. Same as Fig. 4 for the Type IIa problem when $p = 0$.

at the left boundary only, obtaining equation (39a), below; and retain the previous Type IIb BC's at the bottom. These are perfect BC's for both physical and spurious Type II trigonometric modes.

The normal $(x)$ equation at the left is identical to that enforced in the Type I problem. Hence, the blend of physical and spurious modes expressed in (27) is exactly the same! Thus, the $\alpha_1/\alpha_2$ ratio shown in Fig. 3 pertains to both Type I and Type IIa problems. The actual $\alpha$ values dictated by the two problems, however, are different. Fig. 12 shows the $p = 0$ Type IIa problem solution for the same set of $(\gamma h)^2$ and $(kh)^2$ parameters used in Fig. 4. The parasitic mode is again a significant fraction of the total solution having grossly erroneous behavior similar to Fig. 4, but with different local details.

For the special case $p = 1$, a single mode of the form (37) is sufficient, and the normal $(x)$ equation demands the same relation for $f$ as in the Type I problem, equation (31) which has the same accuracy shown in Fig. 5. The tangential BC on the left gives $\alpha$

$$\alpha = \frac{\frac{iA_y k^2}{\gamma}}{i\gamma B_y f + \frac{h}{2} A'_x\left(C_y^2\gamma^2 - A_y k^2\right) - i\sigma B'_x A_y}. \tag{40}$$

The product $\alpha f$ is unity for the analytic solution. Fig. 13 reveals that (40) can be a gross distortion of this feature at reasonable resolution. The left BC's in this case are singular for certain combinations of $k^2$ and $\gamma^2$, at which point $\alpha f$

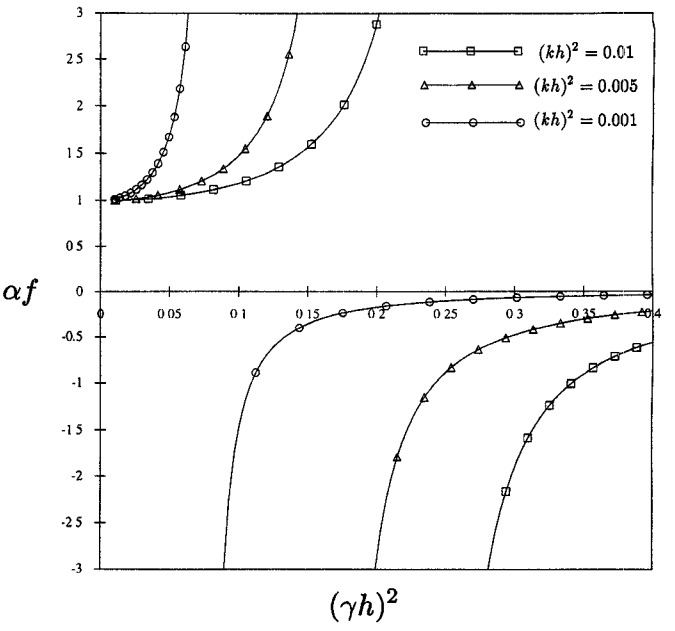


Fig. 13. $\alpha f$ for the Type IIa $p = 1$ solution as a function of $(\gamma h)^2$. The exact value is unity.

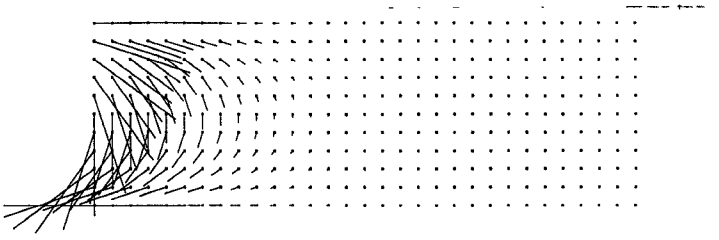

Fig. 14. Same as Fig. 11 except Type IIa BC's are enforced on the left.

goes to infinity. For larger $\gamma^2$, $\alpha f$ becomes negative and the field is wrong in both magnitude and direction. For complex problems, this is a particularly bad feature, since the basic waveform has the correct dispersion relation and mode shape $f$. Fig. 14 displays the $p = 1$ solution for the case reported in Fig. 11, illustrating this point. Here, $\alpha f = -1.5788$.

Finally, consider the Type IIa BC at the bottom, equation (39b) below.

The tangential $(x)$ equation is transparent to the Type II trigonometric modes as above; it serves only to constrain the ratio $E_x/E_y$ for the Type I modes (which are required by the left BC to vanish). The normal $(y)$ equation is critical.

$$\sum_l \begin{bmatrix} \frac{1}{2} A'_x C_y^2\gamma^2 - \frac{p}{h} i\sigma B'_x A_y - \frac{1}{2} A'_x A_y k^2 & i\gamma B_y\left(\frac{i}{2}\sigma B'_x - \frac{p}{h} A^*_x\right) \\ i\gamma B_y\left(\frac{1}{h} A^*_x - \frac{ip}{2}\sigma B'_x\right) & \frac{p}{2} A'_x C_y^2\gamma^2 - \frac{1}{h} i\sigma B'_x A_y - \frac{1}{2} A'_x A_y k^2 \end{bmatrix}_l \begin{Bmatrix} E_x \\ E_y \end{Bmatrix}_l = \begin{Bmatrix} 0 \\ -\frac{1}{\gamma h} A_y k^2 \sin\gamma y \end{Bmatrix} \tag{39a}$$

$$\sum_l \begin{bmatrix} \frac{p}{2} A'_y C_x^2\sigma^2 - \frac{1}{h} i\gamma B'_y A_x - \frac{1}{2} A'_y A_x k^2 & i\sigma B_x\left(\frac{1}{h} A^*_y - \frac{ip}{2}\gamma B'_y\right) \\ i\sigma B_x\left(\frac{i}{2}\gamma B'_y - \frac{p}{h} A^*_y\right) & \frac{1}{2} A'_y C_x^2\sigma^2 - \frac{p}{h} i\gamma B'_y A_x - \frac{1}{2} A'_y A_x k^2 \end{bmatrix}_l \begin{Bmatrix} E_x \\ E_y \end{Bmatrix}_l = \begin{Bmatrix} 0 \\ 0 \end{Bmatrix}. \tag{39b}$$

It is transparent to the Type I modes, and *overconstrains* the Type II modes. Specifically, it requires that both physical and spurious modes independently satisfy a mode shape requirement $f_i'''$ which is incompatible with the interior equations. For $p = 0$ and after some manipulation[3], this is

$$f_i''' = \frac{4}{6}\left(\frac{B_y\left(C_x^2\sigma^2 - A_x k^2\right)}{B_x \sigma\gamma C_y^2}\right)_i \tag{41}$$

for both $i = 1, 2$. But this conflicts with the interior equations which have already determined $f_1$ and $f_2$. Each mode therefore demands an additional parasite $(\sigma_1, \gamma_1)$ and $(\sigma_2, \gamma_2)$ in addition to the original parasite $(\sigma_1, \gamma)$ and the physical mode $(\sigma_2, \gamma)$. These will be blended to meet the bottom BC's in a manner analogous to that used at the left. Further, the additional spurious $\gamma_1$ and $\gamma_2$ in the system will create imbalances in the left BC's; each will demand an additional parasitic mode; and so on. This basic conflict between $f'''$ and $f$ is not improved with mesh refinement; for $p = 0$, we have

$$\frac{f_i'''}{f_i} = \frac{4}{6}\frac{B_y^2}{C_y^2 A_y} \tag{42}$$

which converges to $4/6$. We see no simple closure of this broadening spectrum of parasites.

For the case $p = 1$, the normal equation at the bottom can be seen to be in direct conflict with the normal equation at the left. For a Type II mode of the form (37), we have

$$f = \frac{\gamma B_y}{\sigma B_x}\left(h^2\,\frac{\left(C_x^2\sigma^2 - A_x k^2\right)}{6} - A_x\right). \tag{43}$$

This is different from and incompatible with (31) which results from the left normal BC, except in the limit of small $h$ where both converge to the same analytic value. For a finite mesh, therefore, we find no solution for $p = 1$ with Type IIa BC's.

## VI. Discussion

We have analyzed in detail the imposition of boundary conditions on discrete finite element equations at mesh terminations. Coupling these with previously obtained dispersion relations on the interior allows closed-form solutions for driven boundary value problems on simple meshes. We have concentrated on node-based, $C^\circ$ elements because of their widespread use in other applications, and their well-known ability to support spurious vector parasites.

Relative to double-curl formulations, we concluded in [7] that spurious modes would necessarily be required to satisfy physical boundary conditions. The present analysis confirms this in detail and quantifies the strength of the parasite. The examples shown are reminiscent of numerical results reported in [9] for more complex geometries—demonstrating the power and generality of the present idealized findings. Both Type I and Type IIa BC's yield unambiguously poor results with the double-curl form. The Type IIb condition, although seldom used with the double-curl equation, retains the parasite even though in the examples chosen here it is quite small. This may represent a limited window of utility for the double-curl method on $C^\circ$ elements.

By contrast, the Helmholtz solutions are of high quality for Type I and IIb BC's. These findings are consistent with numerical experiments in [9] and in [8]. These papers deal with two alternative Helmholtz forms which reduce to the homogeneous form analyzed herein. In [3], we provide a very general derivation of Helmholtz-like weak forms based in gauge theory, which significantly broadens their foundation and demonstrates the sufficiency of both Type I and IIb BC's.

The Type IIa conditions should be avoided when using the Helmholtz forms. This BC blend is shown herein to overconstrain the Helmholtz system—effectively it demands two slightly different and incompatible approximations to $\nabla \cdot \boldsymbol{E} = 0$. This finding is compatible with the computational experience reported in [9]. A reexamination of the problematic cases presented therein (Fig. 5 and 6) reveals very ill-conditioned system matrices with Type IIa BC's; and a condition number reduction of order $10^3$ for Type IIb BC's.

These analyses indicate that simple node-based finite elements are capable of supporting robust, high-quality solutions to Maxwell's equations, provided the Helmholtz-type weak forms are used with appropriate boundary conditions.

[3]The mode summation for the bottom BC must be performed by breaking the trigonometric modes into their exponential parts in order to accommodate the one-sided discretization factors.

## References


[1] I. Bardi, O. Biro, and K. Preis, "Finite element scheme for 3D cavities without spurious modes," *IEEE Trans. Magn.*, vol. 27, pp. 4036–4039, 1991.

[2] A. Bossavit, "Solving Maxwell equations in a closed cavity and the question of spurious modes," *IEEE Trans. Magn.*, vol. 25, pp. 702–705, 1990.

[3] W. E. Boyse, D. R. Lynch, K. D. Paulsen, and G. N. Minerbo, "Nodal based finite element modeling of Maxwell's equations in three dimensions," *IEEE Trans Antennas Propagat.*, vol. 40, pp. 642–651, 1992.

[4] Z. J. Cendes and P. P. Silvester, "Numerical solution of dielectric loaded waveguides: I—Finite element analysis," *IEEE Trans. Microwave Theory Tech.*, vol. MTT-18, pp. 1124–1131, 1970.

[5] D. G. Corr and J. B. Davies, "Computer analysis of the fundamental and higher order modes in single and coupled microstrip," *IEEE Trans. Microwave Theory Tech.*, vol. 20, pp. 669–678, 1972.

[6] J. F. Lee, D. K. Sun and Z. J. Cendes, Tangential vector finite elements for electromagnetic field computation," *IEEE Trans. Magn*, vol. 27, p. 4032–4035, 1991.

[7] D. R. Lynch and K. D. Paulsen, "Origin of vector parasites in numerical Maxwell solutions," *IEEE Trans. Microwave Theory Tech.*, vol. 39, pp. 383–394, 1991.

[8] K. D. Paulsen, W. E. Boyse, and D. R. Lynch, "Continuous potential Maxwell solutions on nodal-based finite elements," *IEEE Trans. Antennas Propagat.*, 40, 10, 1192–1200. 1992.

[9] K. D. Paulsen and D. R. Lynch, "Elimination of vector parasites in finite element Maxwell solutions," *IEEE Trans. Microwave Theory Tech.*, vol. 39, pp. 395–404, 1991.



**Daniel R. Lynch,** photograph and biography not available at the time of publication.

**Keith D. Paulsen,** photograph and biography not available at the time of publication.

**William E. Boyse,** photograph and biography not available at the time of publication.